Faculty of Medical and Health Sciences, University of Poonch Rawalakot
Journal of Pharma and Biomedics
ISSN: 3007-1984(online), 3007-1976 (Print)
https://www.jpbsci.com/index.php/jpbs

Exploring the Role of EGCG as Aβ-42 Inhibitor: An in Silico Study on hIAPP Octamer Destabilization

Hina Afshan, Javeria Inam, Waqas Afzal, Rabbia Adil, Beenish Khurshid*

Department of Biochemistry, Faculty of Chemical and Life Sciences, Abdul Wali Khan University, Mardan, Pakistan.

Received: May 20, 2025; *Revised: June 29, 2025;* *Accepted: June 30, 2025*

A B S T R A C T

Amyloid beta is an abnormally folded protein that aggregates in the lipid bilayers of brain cells. This causes structural disruption in the brain, contributing to Alzheimer's disease. It exists in various forms, starting as monomers, oligomers (including dimers, trimers, tetramers, and more). It then aggregates into protofibrils and, finally, fibrils. Of these, Aβ-42 is more toxic than Aβ-40, making it a significant target for Alzheimer's research. Strategies that disrupt Aβ-42 may provide potential treatments for AD. At present, natural compounds are emerging as a focus in combating toxic compounds involved in neurodegenerative disease. The presence of diverse functional groups and distinct molecular structures contributes to therapeutic potential. Among the catechins present in green tea extracts, epigallocatechin-3-gallate (EGCG) exhibits the strongest antioxidant property. This highlights its potential in neuroprotective drug discovery. In this work, we performed the molecular dynamics simulations to investigate the molecular interactions between EGCG and the target hIAPP. In the first part, we did a comparative analysis of widely used force fields. It was found that the CHARMM-27 force field is most reliable for maintaining the beta-sheet organization. In the second part of the study, a 200 ns simulation revealed that EGCG forms various strong binding interactions with the hIAPP, resulting in disruption of its beta-sheet structure. The hydroxyl groups and aromatic rings of EGCG interact with the hIAPP more firmly. It disrupts the intra-peptide bonds of protein structure. The structural features and biochemical activity of EGCG make it a promising lead compound. It can be used to create novel, potent, and effective analogues to treat Alzheimer's disease.

Keywords: Disease, EGCG, Amyloid beta, Neurodegeneration, Molecular dynamics, Aggregation inhibition.

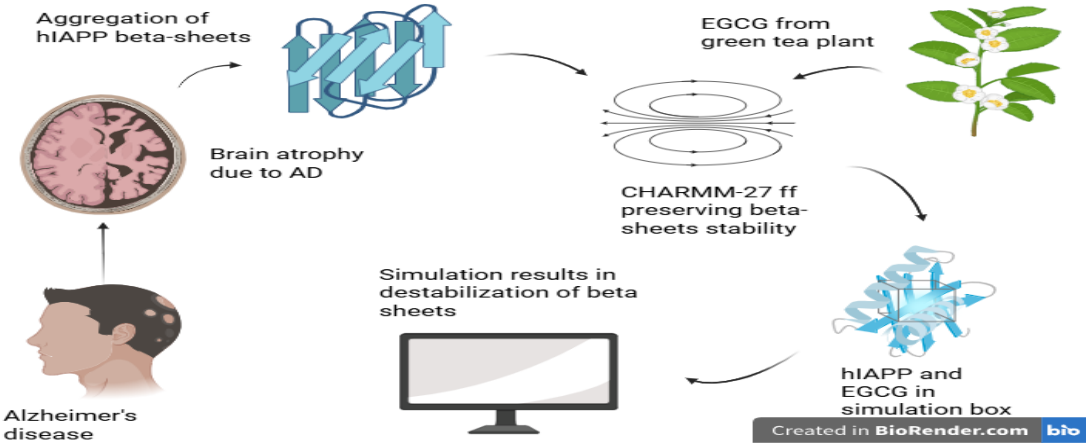

Corresponding Author: Beenish Khurshid *
Email: beenish_khurshid@awkum.edu.pk

INTRODUCTION

Neurodegenerative diseases have become one of the main focuses of health. These include mainly Alzheimer's disease and Parkinson's disease (Xie et al., 2014). Alzheimer's disease is a chronic brain-degenerative disorder that is the leading cause of dementia (Kareem et al., 2025). It is caused by progressive brain atrophy, loss of memory, language difficulties, and changes in behavior. Globally, the United Nations health authority listed dementia as the seventh principal cause of death among elderly people (WHO, 2021). It affects women more than men. According to the World Health Organization (WHO), more than 50 million people are living with dementia. Of these, 60-70% of cases are of Alzheimer's disease (Zvěřová, 2019). By 2030 and 2050, the number is expected to reach 78 million and around 150 million, respectively (15th March, 2023 report of WHO).

Different hypotheses have been proposed to explain Alzheimer's disease. The most widely accepted one is the amyloid beta hypothesis (Paroni et al., 2019). It follows two pathways: the amyloidogenic pathway and the non-amyloidogenic pathway. Amyloid beta peptides are produced through the amyloidogenic pathway (Hida et al., 2025). This process starts when Amyloid Precursor Protein (APP) is cleaved by beta-secretase. This forms an extracellular fragment (soluble) and a membrane-bound fragment (C99). Gamma-secretase further cleaves the C99 fragment, resulting in the formation of Aβ peptides. These peptides are of various lengths, ranging from 37 to 42 amino acids (Coronel et al., 2023). Aβ-42 is more prone to aggregation, leading to oligomer formation. These oligomers grow into protofibrils and then insoluble fibrils. Fibrils disrupt the neuronal networks and signaling. This leads to impaired memory and decline in cognitive functions, the key symptoms of Alzheimer's disease. Aβ-42 fibrils contain a higher content of beta sheets as compared to Aβ-40 (Lee et al., 2019). Additionally, these fibrils occur in the form of parallel and antiparallel or cross sheets (Chaachouay and Zidane, 2024). Misfolding into these beta sheet-rich conformations is the leading cause of amyloidogenesis.

For decades, researchers have been looking for effective inhibitors to stop or slow down the disease progression. Although the failure of many inhibitors is due to their inability to cross the blood-brain barrier and huge side effects on other body organs. Compounds derived from natural products often provide stability and safety (Chaachouay and Zidane, 2024). They are biologically more compatible than many other synthetic drugs that have side effects and are of higher cost. These can halt Aβ fibrillization by the action of aggregate disruption (Xu et al., 2023). This includes many small molecules, peptides, and proteins. Scientists have been working on a vast list of polyphenols. These are flavonoids and terpenoids, including curcumin, resveratrol, quercetin, myricetin, rosmarinic acid, and many more. These compounds exhibit strong antioxidant and anti-inflammatory properties, thereby destabilizing fibril formation (Sedov and Khaibrakhmanova, 2022).

A group of natural polyphenols, particularly epigallocatechin-3-gallate (Camellia sinensis), are abundantly found in green tea. It is primarily extracted from the leaves of green tea. EGCG contains 50-80% of total tea catechins. One cup of green tea having 2.5 mg contains 130 to 180 mg of EGCG (Baldi et al., 2020). It first originated in China and widely spread from Asia to Western Europe (Pan et al., 2022). The various key reasons for choosing EGCG are that it has low toxicity and is safe at normal concentrations. It can cross the blood-brain barrier and also interrupts cellular senescence (Khalifa et al., 2024). Besides these properties, EGCG also affects gene expression via DNA methylation or histone modification. It prevents oxidative damage (metal-catalyzed) and is environmentally friendly. Moreover, EGCG promotes cancer suppression. It affects several cellular pathways, especially the MAPK (Mitogen-Activated Protein Kinase) pathway. It is also involved in atherosclerosis, obesity, and type 2 diabetes (Liu et al., 2024).

The green tea catechin has a molecular weight of 458.4 g/mol. It can interact with many molecules because of its chemical structure. EGCG contains a catechol group—a benzene ring with two hydroxyl groups and a gallate group, a gallic acid derivative. The gallate ester forms hydrogen bonds and π–π stacking interactions with other biomolecules (Bu et al., 2024). This is due to its various hydroxyl groups and the presence of aromatic rings. The hydroxyl groups at the positions 3, 4, and 5 on the rings enhance its antioxidant properties (Karakuş, 2024). This compound is a highly polar molecule but neutral at physiological pH. EGCG does not carry any charges; however, at very high or low pH, it undergoes partial ionization. Thus, it has the ability to disintegrate the Aβ fibrils.

Before running the simulation of hIAPP with EGCG, we first analyzed three different force fields. The goal was to find the most effective force field for stabilization of beta sheets, crucial for understanding Alzheimer's disease. The selected force fields were AMBER96SB-ILDN, CHARMM-27, and GROMOS96-54a7. These force fields

were selected based on their better performance in earlier studies in modeling Aβ-42 fibrils (Nirmalraj et al., 2024). The water model used for both AMBER96SB-ILDN and CHARMM-27 was the TIP3P. GROMOS96-54a7 was used in combination with SPC. A 200 ns simulation was run with each force field. As a result, CHARMM-27 performed best at maintaining the beta sheets in all three force fields.

In this research study, the effect of EGCG on hIAPP was studied by means of molecular dynamics simulations. The main aim is to reveal atomistic details of binding interactions between these two molecules. Our simulations showed that EGCG caused significant changes in the hIAPP and destabilized the secondary structure into a disordered conformation. Also, it formed hydrogen bonding, hydrophobic interactions, and π–π stacking interactions with the EGCG. This involved the core domain, NFGAIL-S, of hIAPP. Identifying the exact mechanism of action of EGCG with the hIAPP will better illustrate its binding interactions and disruptive behavior (Mo et al., 2016). The findings could help design catechin-based effective inhibitors against hIAPP Aβ-42 buildup. This study can also provide direction for future experimental investigation, aiding in drug development.

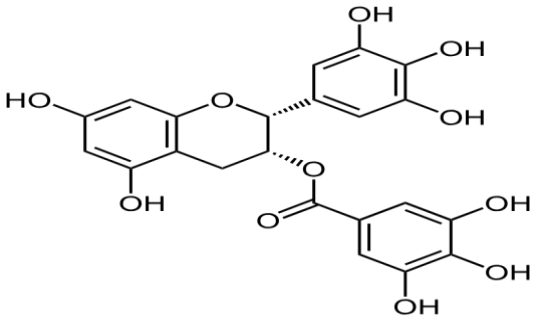

Figure 1: EGCG contains four aromatic benzene rings that facilitate the hydrophobic interactions with the hIAPP protein structure.

Straasø et al. (2014) successfully determined the atomic structure of the protein fibril (2KIB) using solid-state NMR spectroscopy. The fibril structure of the SNNFGAILSS fragment was identified from human islet amyloid polypeptide (Li et al., 2024). This was done with an accuracy of about 0.52 Å resolution. It was revealed to be an octameric with 8 chains containing beta-sheets. Also, it contained a total of 56 residues and 5.77 kDa of structural weight.

An in vitro experiment was performed by Cano et al. (2019) on APP/PS1 transgenic mice. It revealed that 40 mg/kg of EGCG or nano EGCG was administered for almost 3 months. This led to strong suppression of Aβ fibrillation. One of the in vivo experiments was conducted by the PENSA study group in October 2019 in Barcelona, Spain. This group used a dose of 520 mg EGCG per day to find out whether memory decline slows down in elderly people. The trial was specified for people with a higher risk of AD due to the APOE4 gene. A total of 200 participants participated in this experiment and were split into four groups. This study was completed in one year. Zhang et al. (2020) demonstrated by performing MD simulations how EGCG interacts with the Aβ-42 protofibril. They showed that its disruptive mechanism is only due to strong hydrogen bonds) (Xue et al., 2025). It also contained an extra gallic acid ester group that provides additional hydroxyl groups. In addition to this, it has increased affinity for metal chelation. According to the same group, this compound disrupted the hydrogen bonds and salt bridges, essential for maintaining the fibril structure. Li et al. (2021) observed that the ring GA (gallic acid) of EGCG forms cation-π interactions with Aβ-42 protofibril, leading to its disruption.

Li et al. (2024) demonstrated that EGCG effectively reduces the interactions between Aβ and hIAPP within their heterodimers. These inter-chain and intra-chain interactions were reduced through aromatic interactions. This group also showed by replica exchange MD simulations that the beta-sheet structures within the core regions of this complex were diminished. This resulted in the shifting of the sheets to coiled structures.

METHODOLOGY

Using the GROningen MAchine for Chemical Simulations (GROMACS) version 2022.4, MD simulations were performed. We conducted two sets of simulations, one in water only and another one with a ligand. First, we took the structure of the fibrillar Aβ-42 octamer from the Protein Data Bank (PDB ID: 2KIB). This structure was resolved using solid-state NMR spectroscopy. The molecular structure of the chemical compound, Epigallocatechin-3-

gallate, was obtained from the ChEMBL database (ID: CHEMBL297453). The parameters of EGCG were generated from SwissParam. The CHARMM-27 force field was used to parameterize the hIAPP. The water model selected was TIP3P (Transferable Intermolecular Potential with 3 Points)**.** Both systems of hIAPP and hIAPP-EGCG were simulated using the same protocol. First, we converted the PDB file of hIAPP into a GROMACS-compatible gro file. The hIAPP is placed in the center of a cubic box.

The distance between the peptide and the box edge was 1.0 nm (the sides of the box were 5.39472 × 5.39472 × 5.39472 nm). 4748 TIP3P water molecules were used to solvate the system. Here, SPC216 was used for solvent configuration of TIP3P, as it is a three-point water model. The overall charge is neutralized by adding 14 Na^+ and 14 Cl^- so that a 150 mM NaCl concentration is achieved, which is close to the physiological value. Using the steepest descent algorithm, the system was energy minimized for a maximum of 50,000 steps (100 ps). The step size kept was 0.01 nm, with a maximum force applied to each atom in the system of less than 1000.0 kJ/mol/nm. For buffered neighbor searching, the Verlet cutoff scheme was used. The system was then equilibrated for 100 ps in the NPT ensemble. The temperature was controlled at T = 300 K using a velocity rescaling thermostat (modified Berendsen). 0.1 ps was used as a coupling time constant.

The equilibration of pressure is performed under the NVT ensemble for 100 ps at P = 1 atm using the Parrinello-Rahman barostat. The coupling time constant was kept at 0.2 ps. A 1.0 nm cutoff was used for both short-range coulombic and van der Waals interactions. It utilized the Periodic Boundary Conditions (PBC) in all three directions (Zhu et al., 2023). For both NVT and NPT, the log file was updated every 1.0 ps. The atomic bonds of molecules involving only hydrogen atoms were restrained using the LINCS (Linear Constraints Solver) algorithm. For the calculation of electrostatic forces, the Particle Mesh Ewald (PME) method was used. The final MD run was performed at a constant temperature of 300 K and a pressure of 1 atm for 200 ns. A time step of 0.002 ps was used for each simulation step. Configurations were saved after every 200 ps. Using the VMD package, the obtained trajectories were visualized. These were analyzed by utilizing the GROMACS tool, like Xmgrace.

Table 1**:** Modeling and simulation details for all-atom MD of hIAPP and hIAPP-EGCG systems.

System	Aβ-hIAPP	Aβ-hIAPP-EGCG
Simulation time	200 ns	200 ns
Box size	5.39521 × 5.39472 × 5.39472 nm	5.39521 × 5.39521 × 5.39521nm
Number of water molecules	4748	4726
Number of ions (Na+, Cl-)	14, 14	14, 14
Temperature	300 K	300 K
Pressure	1 atm	1 atm
Number of atoms	15093	15149

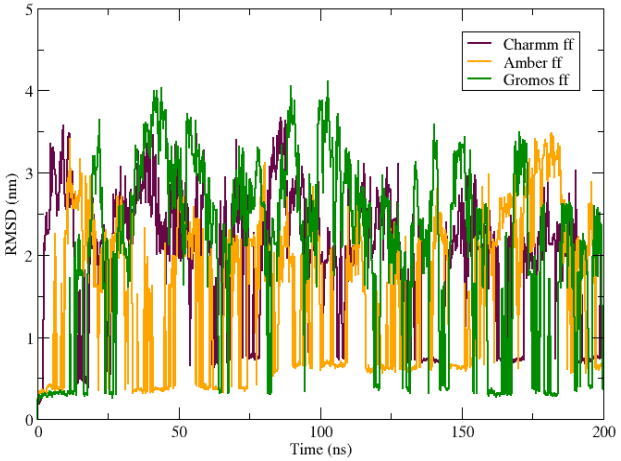

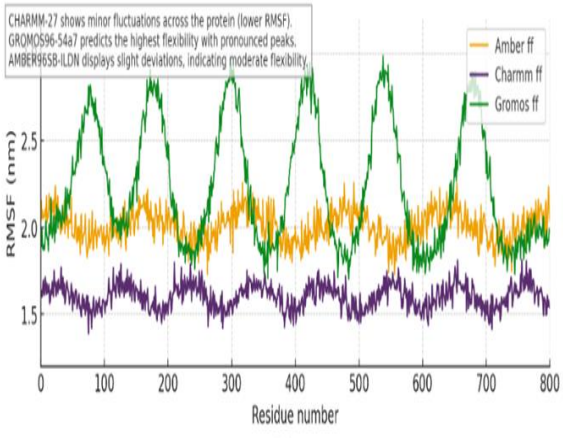

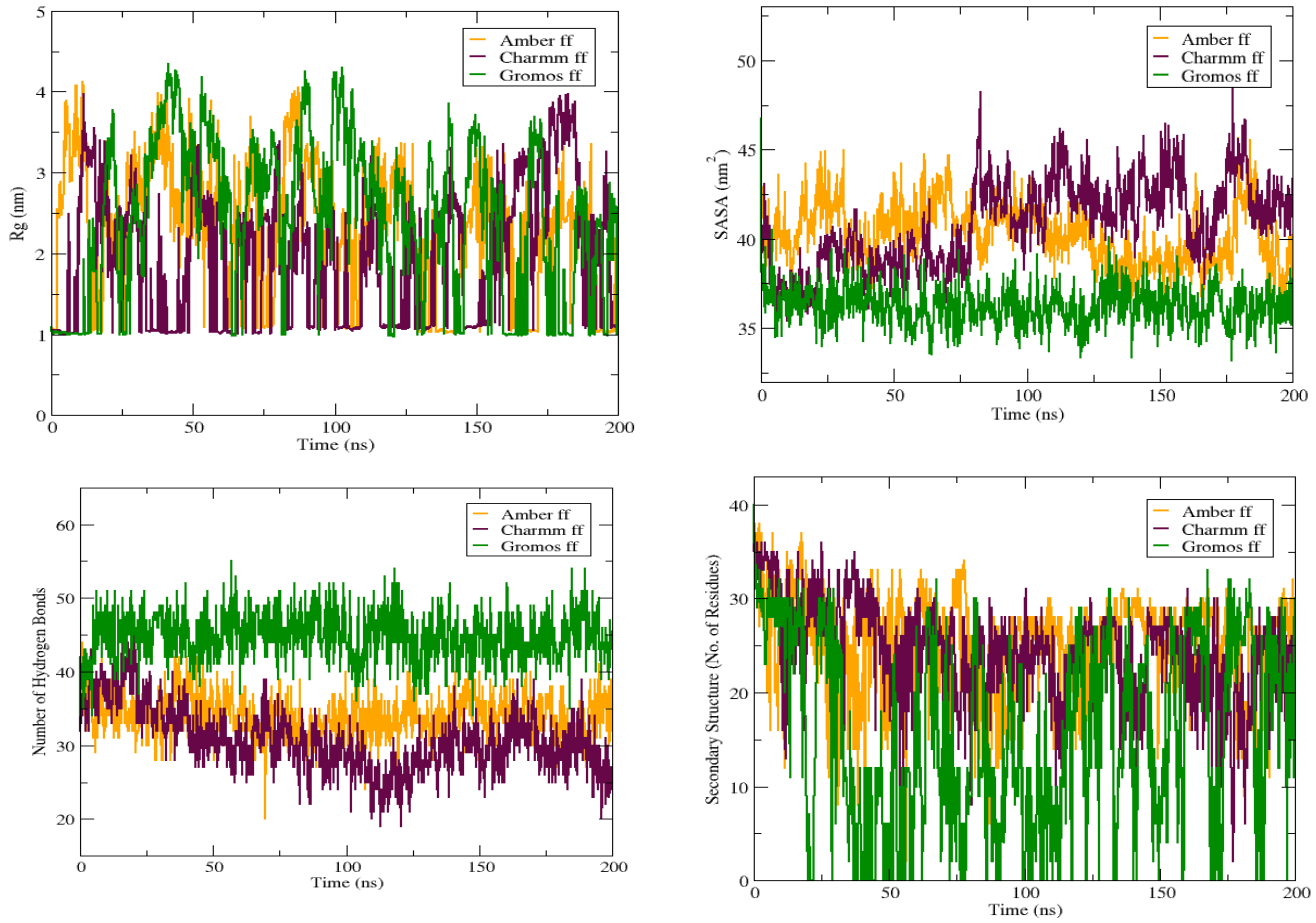

Figure 2: (a) RMSD graph illustrates that CHARMM-27 produced the most stable hIAPP structure, with lesser deviations. GROMOS96-54a7 exhibits greater deviations, indicating less stability. AMBER96SB-ILDN presents an intermediate structure between the two. (b) The RMSF plot shows minor fluctuations across the protein in CHARMM-27. GROMOS96-54a7 predicts the highest flexibility. AMBER96SB-ILDN displays slight deviations, indicating moderate flexibility. (c) The value of Rg for CHARMM-27 is low, revealing a more compact hIAPP structure throughout much of the simulation. GROMOS96-54a7 shows higher Rg, predicting a more expanded protein structure. AMBER96SB-ILDN also displays higher deviations, suggesting a less exposed conformation as compared to GROMOS96-54a7. (d) CHARMM-27 reveals the highest SASA value, showing a more solvent-exposed structure. GROMOS96-54a7 exhibits less variability as compared to the other two force fields. AMBER96SB-ILDN fluctuates moderately over time, indicating dynamic exposure of buried sites. (e) For CHARMM-27, the number of hydrogen bonds ranges from 20 to 45. AMBER96SB-ILDN shows a lower range of hydrogen bonds, approximately 20 to 42. GROMOS96-54a7 depicts a greater number of hydrogen bonds, fluctuating between about 36 and 55. (f) The secondary structure graph illustrates high spikes and frequent decreases to low residue numbers for the GROMOS96-54a7 force field, highlighting a less stable structure. CHARMM-27 depicts more secondary structure elements, with overall less fluctuation over time. AMBER96SB-ILDN shows an intermediate conserved structure.

Force Fields Analysis

The force field plays a crucial role in sustaining the stability and consistency of molecular dynamics simulation. It sets the rules for atomic interactions, influencing how atoms in a protein move and maintaining native structure. Differences in force field variables affect the simulation outcomes. To investigate the effect of a force field on the MD simulation of hIAPP, we performed a comparative analysis using the AMBER96SB-ILDN, CHARMM-27, and GROMOS96-54a7. The main objective is to identify the most suitable force field for stabilizing the beta-sheets of hIAPP over simulation time. These results can help improve the simulation outcomes of hIAPP. For each force field, six different parameters were analyzed.

Table 2: Details of MD setup for various force fields.

Force fields	AMBER99SB-ILDN	CHARMM-27	GROMOS96-54a7
System	Aβ-hIAPP	Aβ-hIAPP	Aβ-hIAPP
Water model	TIP3P	TIP3P	SPC
Box type	Cubic	Cubic	Cubic
Simulation time	200 ns	200 ns	200 ns

Although CHARMM-27 revealed a moderate number of hydrogen bonds. But it persistently formed a more stable and condensed structure across all analyzed parameters. This indicates its high stability for simulating hIAPP. The GROMOS96-54a7 force field displayed higher fluctuation, indicating more flexibility. AMBER96SB-ILDN presented intermediate behavior to the two.

RESULTS

MD simulation is a robust and reliable modeling technique. It is used to investigate the overall physical characteristics of systems occurring due to variable molecular interactions. In this research, we chose two molecular setups for simulation: the protein in water and the protein with ligand for about 200 ns each. We used various tools to analyze the changes in the protein structure as it approached disruption. These include the Root Mean Square Deviation (RMSD), Root Mean Square Fluctuation (RMSF), hydrogen bond, and secondary structure analysis. The analyses were conducted using built-in algorithms and GROMACS tools. The findings showed that the hIAPP binds tightly with EGCG. This highlights the interference of EGCG to inhibit the formation of toxic amyloid deposits.

Trajectory Analysis

Å between the LIG-8 and Gly-3 and Asn-1, respectively. (c) At the final 200 ns, a distance of 4.09 and 4.63 Å between LIG-8 and Leu-6 and Ser-7 indicated good results. It showed that the ligand remained intact in the binding pocket of hIAPP. This illustrates the stability of the complex through the formation of binding interactions.

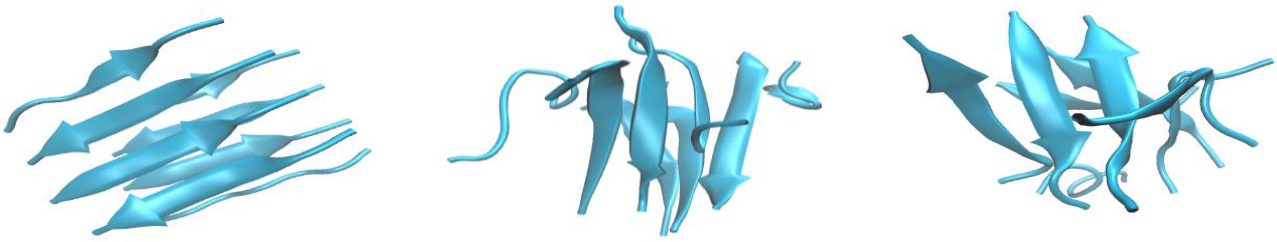

Figure 3: (a) Snapshots of the MD trajectory of hIAPP in water were extracted at some simulation phases. At 0 ns, the hIAPP was in its native state after energy minimization and equilibration, and no major unfolding of structure occurred. (b) At 100 ns, slight fluctuations indicated adjustments of specific regions as a result of exposure to water. This showed structural flexibility of hIAPP. (c) At the end of the simulation, the overall structure of hIAPP remained stable with no primary disruption. It also highlights the consistency of the CHARMM-27 force field as well to preserve the beta sheets.

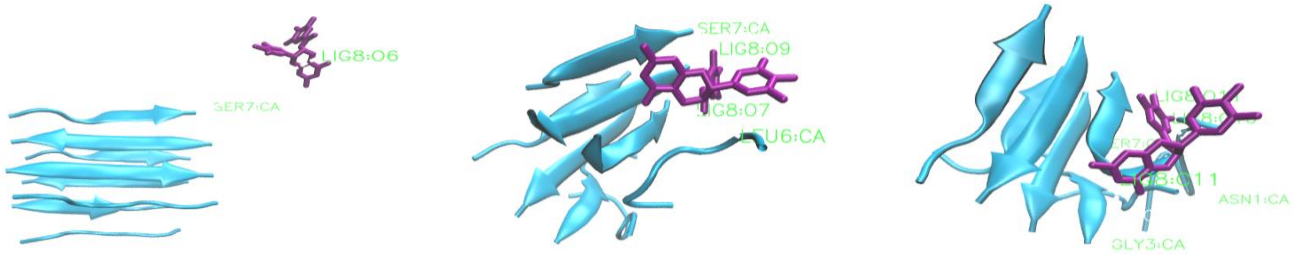

Figure 4: (a) Snapshots of the hIAPP and EGCG complex were taken at 0 ns, 100 ns, and 200 ns to observe the MD trajectory after ligand binding. At 0 ns, the EGCG was at its initial position before the simulation started, with a distance of 14.65 Å between Ser-7 and LIG-8. (b) In the middle of the simulation, minor changes in the hIAPP structure highlighted its flexibility around the EGCG. It is also shown by the lesser distance of 10.62 and 11.51 Å between the LIG-8 and Gly-3 and Asn-1,

respectively. (c) At the final 200 ns, a distance of 4.09 and 4.63 Å between LIG-8 and Leu-6 and Ser-7 indicated good results. It showed that the ligand remained intact in the binding pocket of hIAPP. This illustrates the stability of the complex through the formation of binding interactions.

Structural Dynamics of Complex

Root Mean Square Deviation

RMSD analysis is used to track how much the atoms in the system move away from their original coordinates during the simulation. These results provide information about the structural stability of the complex or conformational changes occurring in the protein. As the selected protein (2KIB) is an hIAPP fibril, a highly stable moiety, any changes in the RMSD lead to alterations in its stability. We compared the RMSD of the protein alone to that of the protein-ligand complex to assess the structural differences. At the start of the simulation, there is an initial rise in RMSD of both systems, the hIAPP protein and the EGCG-hIAPP complex. It was observed due to the equilibration and kinetic energy distribution of the systems. The average RMSD value over backbone atoms ranged from 2.0 to 2.5 nm for protein and 2.5 to 3.0 nm for the complex. The value reached 3.0 and 3.6 nm for the initial 20 ns, showing structural adjustments for the protein and complex, respectively. The hIAPP showed sharp fluctuations throughout the simulation. It reached up to 3.5 nm, indicating unstable behavior. The RMSD of the complex has fewer fluctuations and reached up to 3.8 nm. It plateaued after around 100 ns but showed peaks again from 130 to 170 ns. The transitions are smoother than in the hIAPP, indicating less structural disruption and high stability. It means that the structure maintains its stability on its own. As evident from the studies, hIAPP maintains a stable beta-sheet-rich conformation, making it a potential target for drug design.

Root Mean Square Fluctuation

The RMSF tool was used to determine the fluctuations of residues and flexibility of backbone atoms from their original position upon hIAPP binding. In both systems, the RMSF values of terminal residues were higher, revealing higher flexibility. It was due to the absence of adjacent residues to stabilize the ends of the protein. The graph reflected that the average value ranges from 1.7 nm to 1.8 nm for hIAPP, while in the presence of hIAPP, RMSF ranged from 1.8 to 2.0 nm. This increase in average value refers to the changes in structural rearrangement of residues of the active site. The residues 174-194, 195-206, 504-515, 516-531, and 531-534 showed higher fluctuations. These can form interactions with the EGCG. Whether EGCG was present or not, a similar trend occurred throughout the simulation. This implies that the protein exhibits overall flexibility.

Radius of Gyration

The Rg evaluation signifies that the compactness of the protein increases as it binds with the EGCG, showing a lesser Rg value. As hIAPP is an amphipathic protein, it contains a hydrophilic region as well as a hydrophobic core. This dual nature allows it to interact with polar and non-polar surroundings. For hIAPP alone, Rg fluctuated markedly between 1 and 4 nm. The Rg value for the EGCG-bound hIAPP complex also fluctuated up to 4 nm with several high spikes at 10-20, 50-100, and around 150 ns. We reason that upon EGCG binding, there come some conformational changes in the active sites of hIAPP. It can be transient destabilization as hIAPP adjusts itself to accommodate the EGCG. The Rg value decreased gradually toward the end of the simulation. This indicated more compactness of the complex without global unfolding of hIAPP. Meaning that the hydrophobic region of hIAPP becomes tight.

Table 3: Statistical summary of structural parameters over simulation time.

Parameter	Aβ-hIAPP	Aβ-hIAPP-EGCG
RMSD	1.58 ± 0.91 nm	2.12 ± 0.74 nm
RMSF	1.71 ± 0.09 nm	1.91 ± 0.13 nm
Rg	1.614 ± 0.813 nm	1.675 ± 0.812 nm
SASA	40.81 ± 2.43 nm²	43.09 ± 1.78 nm²

The mean ± SD is calculated based on the last 200 ns trajectories.

Solvent Accessible Surface Area

SASA analysis measures the total surface area of protein that is exposed to the surrounding solvent. It can usually be water. The average value of SASA ranged from 38 to 44 nm² and 42 to 46 nm² for hIAPP and EGCG-hIAPP, respectively. Both the systems consistently exhibited

higher SASA, up to 49 nm². But the complex implied greater SASA value than hIAPP, indicating more exposed regions during the 0 to 175 ns simulation. Onwards up to 200 ns, the complex still possessed a greater SASA value, preventing compaction of protein and exposure to water. Meaning that some specific regions unfold, exposing the buried residues. Here, the hIAPP is offering more active sites for EGCG to interact with, increasing the chances of stronger binding.

Hydrogen Bond Analysis

The total number of hydrogen bonds between the hIAPP and EGCG was observed throughout the simulation by hydrogen bond analysis. From 0 to 100 ns, only 2 hydrogen bonds were formed. Most of them were quite short-lived; they formed and broke till 50 ns. This is because EGCG was searching for stable binding sites on the hIAPP. Onwards from 100 to 150 ns, these bonds increased in number to 4. Here the stable binding started to build between the hIAPP and the EGCG. In the last 50 ns of simulation, a total of 5 hydrogen bonds were developed, indicating stable and stronger binding. The mean distance of hydrogen bonds was 2.86 nm with a lifetime of 0.156 ps.

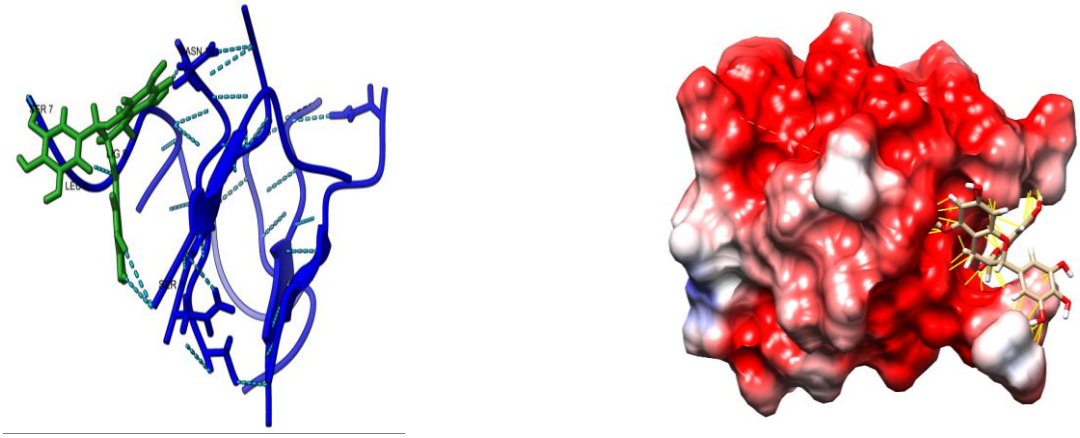

Figure 5: (a) Snapshot of intramolecular hydrogen bonding within EGCG and intermolecular H-bonding with hIAPP. It shows that the Ser, Asn, and Leu are actively taking part in hydrogen bonding with the protein. (b) This figure shows that the EGCG remains intact in the binding pocket of hIAPP by various types of bonding. Here, showing only the Van der Waals interaction with yellow lines. The red portion indicates positively charged residues, while the blue part presents the negatively charged residues of hIAPP. The white region is neutral. It highlights that the bonding residues of protein are mostly positively or zero-charged residues.

Secondary Structure

Secondary structure was investigated using DSSP. Its interpretation signifies the alpha helices, beta sheets, bends, turns, coils, and 3-10 helices. These are produced as a result of interaction between the residues. Initially, the hIAPP started from 36 residues, presenting a more stable secondary structure. The hIAPP-EGCG complex also initiated from 36 residues at 0 ns. But it displayed lower peaks than hIAPP up to 25 ns. This revealed that early structures destabilizes due to hIAPP binding. The hIAPP demonstrated spikes throughout the simulation, but the complex indicated even deeper drops than the hIAPP. This disrupted the structural conformation more. Both the curves decreased over time to even less than 10 residues. Also, it was evident from the secondary structure timeline that the beta sheets were broken down into random coils and turns mostly. This indicated that the EGCG prominently destabilize these aggregating sheets. This analysis clearly revealed disruption of secondary order during the simulation.

Table 4: The averaged secondary structure content of two different systems.

Model system	Coil (%)	β-sheet (%)	α-helix (%)	Bend (%)	Turn (%)
Aβ-hIAPP	28.96 (4.93)	22.59 (5.74)	0.159 (0.774)	2.75 (1.34)	1.11 (1.32)
Aβ-hIAPP-EGCG	31.00 (5.32)	20.56 (5.40)	0.016 (0.252)	2.61 (1.68)	0.90 (1.16)

Data is computed based on the last 200 ns trajectory. The values in parentheses are standard deviations.

Cluster Analysis

Cluster analysis is used to group similar conformations of protein during the simulation. It is based on similarities between the RMSD and helps identify the most dominant and stable structure. A small number of clusters points to the stability of the protein. Similarly, a large number of clusters suggest protein flexibility. During the initial phase (0-26 ns), the number of clusters fluctuated between 2 and 1.5. This illustrated multiple structural states, reflecting the dynamic behavior in the beginning. Meaning that the hIAPP-EGCG complex was unstable initially. After 26 ns, this complex remained in a single cluster, indicating the system has stabilized. The complex now has minimal fluctuations and structural variations, leading to stable interactions of both.

The average cluster size deviated between ~450 and ~900 molecules at the onset of simulation. These fluctuations suggested that the system was not stable and was exploring multiple conformations. It illustrated a transient period of molecular rearrangement, trying to find out a stable mode. Once this size reached approximately 900 molecules, it remained stable from 26 ns afterwards. This plateau portion reflected that the system had acquired stability. It showed high similarity among frames, leading to a more stable structure.

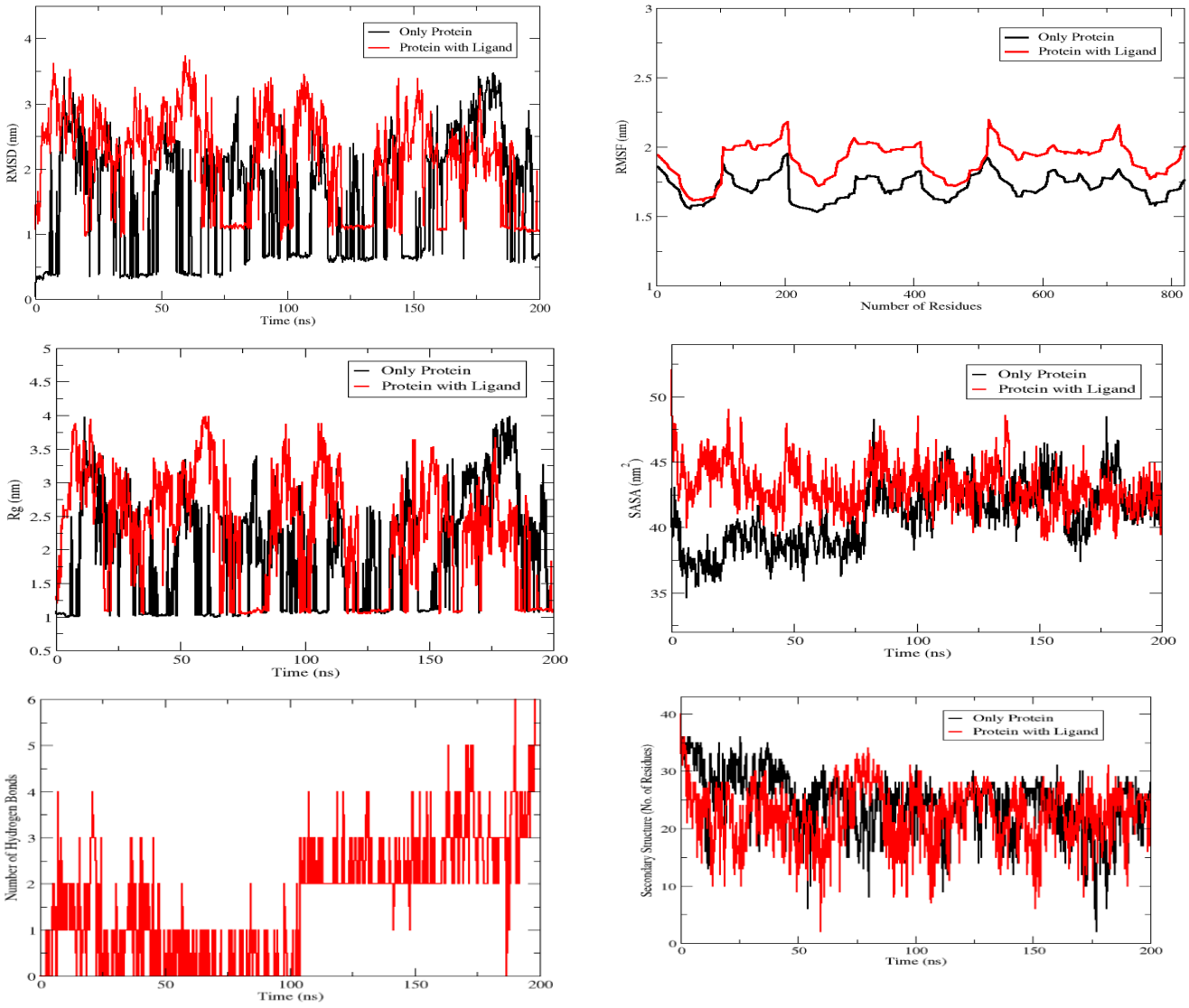

Figure 6: (a) RMSD plot depicting overall high but smoother fluctuations of the hIAPP-EGCG complex compared to hIAPP This indicates structural adjustments and stability of the complex over the simulation time. (b) The RMSF graph per residue represents highly flexible regions of both hIAPP and the complex. The average RMSF is greater for complex, showing the

rearrangement of active site residues after binding of EGCG. (c) The Rg plot reflects more compactness of the hIAPP-EGCG complex as compared to the hIAPP. This shows exposure of a specific binding region, preventing the aggregation of fibril protein. (d) Time evolution of SASA indicates surface exposure to surrounding water. As a result, hydrophilic residues of hIAPP bind to the EGCG, stabilizing the hIAPP-EGCG complex. (e) A greater number of hydrogen bonds in the complex than hIAPP depicts interaction stability. This shows the role of Ser, Asn, and Leu in binding with the EGCG during the simulation trajectory. (f) A time-dependent plot of secondary structure illustrates the loss of stable structure contents of hIAPP upon binding with EGCG. This clearly shows the disruption of secondary conformation over MD simulation.

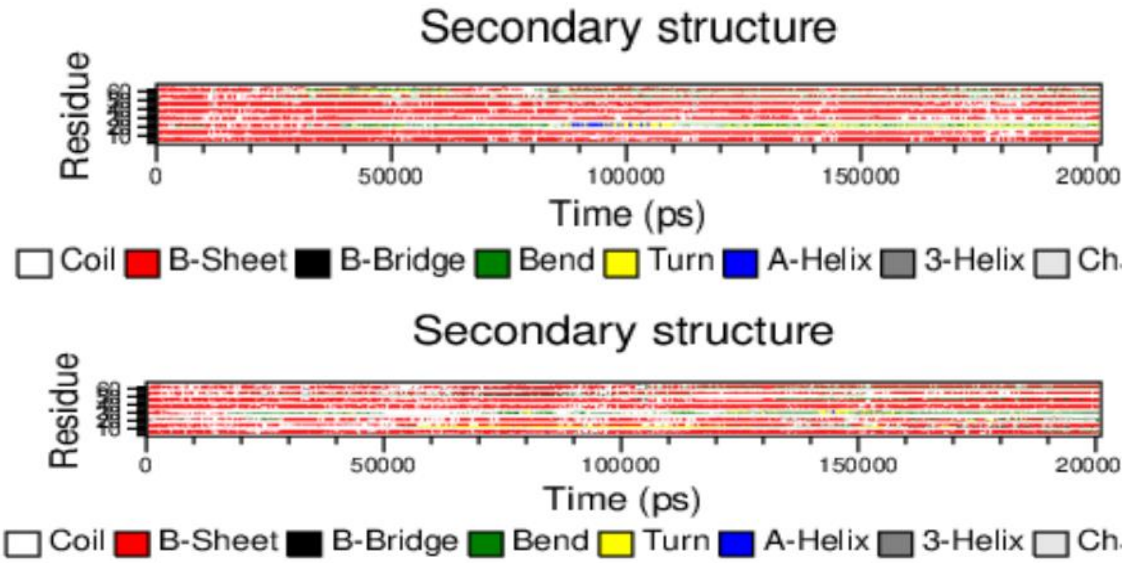

Figure 7: (a) Secondary structure analysis was performed using DSSP. This timeline indicated that hIAPP conserved the beta sheet structure across residues, with fewer transitions explored in bends, turns, and alpha-helix regions. (b) The secondary structure after EGCG binding illustrated that the beta sheets were converted to random coils and bends, increasing their content in the hIAPP. This indicated flexibility of protein structure upon hIAPP binding, destabilizing the protein beta sheets over time.

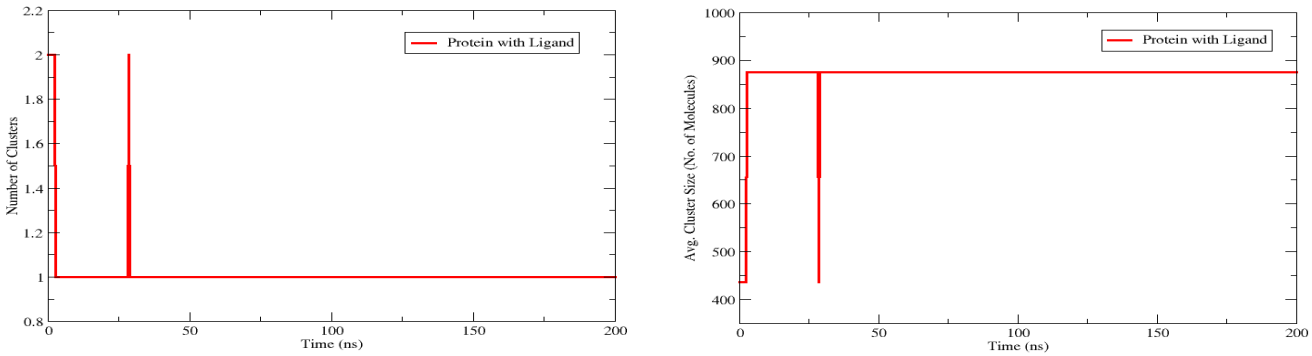

Figure 8: (a) The cluster analysis plot highlights the number of clusters formed during the 200 ns simulation. This number decreases with time to 1, showing the hIAPP-EGCG complex has stabilized. (b) Cluster analysis revealing the size of the cluster, which increases from around 450 to 900 molecules. This depicts that the complex, searching for conformations, has now attained stability.

DISCUSSION

Despite numerous studies, including in vivo and in vitro studies performed on Alzheimer's disease candidates, these drugs remained ineffective. It was due to reduced therapeutic potential and vigorous side effects. Currently, research on natural compounds is a primary focus. But their

interactions are still limited. Therefore, in silico approaches are required to examine these various types of interactions. The main objective of this study was to design a drug that stops the amyloid fibril aggregation by analyzing hIAPP-EGCG interactions. These interactions were explored by utilizing several parameters. The RMSD analysis demonstrated major deviations in the backbone of hIAPP as EGCG binds to it (Wang et al., 2022). It is found out that residues around 5-15, 20-30, and 55-61 (majorly Gly, Asn, Ser, Phe, Leu, Ala, and Ile) showed high RMSD values, affecting the active site's conformation. The higher average RMSD of the complex compared to the hIAPP in the early and mid phases is a significant observation. This is due to deviations at binding sites as a result of its reorganization. This interpretation is further confirmed by RMSF findings. It suggested enhanced flexibility in certain specific regions of hIAPP, indicating structural adaptability of hIAPP. Of particular interest, the Leu (residues 174-194), Ser (residues 195-206 and 504-515), Asn (residues 516-531), and Phe (residues 531-534) revealed higher fluctuations. These form hydrophobic interactions, hydrogen bonds and pi-pi stacking contacts, respectively. A simultaneous increase in the RMSF and decrease in Rg strengthens one of the key concepts. It refers to the fact that localized flexibility occurs within the overall stable structure of hIAPP (Chowdhury et al., 2023). A more compact structural conformation of protein potentially inhibits amyloid fibril formation. In combination with this, increased SASA values imply greater surface exposure. When EGCG binds, it exposes polar residues at the surface pockets of hIAPP but stabilizes the hydrophobic core of it. The beta sheets in the hydrophobic region compact. This suggests that EGCG binds to the hydrophilic residues like Asn and Ser to stabilize the complex. Together, the higher SASA and lower Rg indicate site-specific surface exposure without global unfolding. This clearly shows the targeted exposure to EGCG binding and prevention of aggregation.

From hydrogen bond analysis, we found that EGCCG forms strong hydrogen bonds with polar residues such as Ser-7 and Asn-1. Leu-6, a non-polar residue, also contributes to hydrogen bonding because of its backbone amine and carbonyl groups. It promotes the stability of the hIAPP-EGCG complex and interferes with the inter-peptide hydrogen bonds of hIAPP, which is essential for the growth of fibrils. Changes in secondary structures, particularly the beta-sheets, highlight the ability of EGCG to disrupt the stable amyloid structure (Segura et al., 2024). A reduction in the number of residues from 36 to less than 10, clearly showing the conversion of beta sheets into coils. This points towards the loss of stable structure over the simulation time. The findings from cluster analysis also supported the firm binding of EGCG to hIAPP. It indicates that a single cluster, along with increased cluster size, highlights the broad range of similar shapes within one stable state. This promotes the stabilization of dominant protein conformation over time. Other interactions than hydrogen bonding were also seen. These include π–π stacking interactions formed by the Phe-23 due to its aromatic ring (Jayawardena et al., 2024), while the Gly, Ala, and Ile established the hydrophobic interactions. A total of 55 Van der Waals interactions were developed at a cutoff distance of 4.5 Å. The binding chemistry of hIAPP and EGCG highlights the prominent domain of NFGAIL-S, which is also essential in fibril aggregation of hIAPP. In short, the binding of EGCG with the core segment of NFGAIL-S reveals its power to inhibit the aggregation process. Because this region acts as a binding hotspot for EGCG.

CONCLUSION

In this study, we carried out the molecular dynamics simulations to serve a dual purpose. The first is to assess the influence of commonly used force fields on hIAPP for maintaining the beta sheets. The second is to investigate the binding interactions of EGCG with amyloid fibril, human islet amyloid polypeptide (hIAPP). The results indicate that the CHARMM-27 force field performs best at maintaining the structural stability. Furthermore, the natural molecule EGCG destabilizes the core hydrophobic region of hIAPP by forming strong binding interactions with it. It transforms the ordered state of hIAPP's sheets into a disorganized state. Additionally, residues like Asn-1, Ser-7, Leu-6, and Gly, Ala, Ile, and Phe (NFGAIL-S) play a crucial role in the binding process of EGCG. These form strong hydrogen bonding, hydrophobic interactions, and π–π stacking interactions. This work uncovers the process by which EGCG disrupts the amyloid assembly. It also provides potential insights into the discovery of such compounds with similar efficacy. The major implication is that it supports structure-based drug design for the development of next-generation anti-amyloid drugs. EGCG also acts as a hit compound in the treatment of type 2 diabetes. This study verifies and supports the use of in silico tools like MD simulation in amyloid research. It paves the path for in vivo and in vitro analysis of the activity of EGCG. Moreover, this research identifies the potential binding sites for experimental validation in the future.

A key limitation of this study is the lack of comparative

evaluation of disruption of EGCG with other similar polyphenols. These include the ECG, EGC, EC, and theaflavin found in green and black teas. Secondly, the MD simulation offered valuable molecular insights about hIAPP and EGCG interactions. But experimental validation is necessary to confirm its accuracy and significance. Thirdly, the binding free energies should be calculated to assess the binding efficiency. Moreover, the CHARMM-27 force field has been optimized for the hIAPP and EGCG system. This provided reasonable takeaways in the observed findings. Therefore, the selection of different force fields significantly influences the simulation outcomes.

Conflict Statement

There was no conflict of interest during this study.

REFERENCES

Baldi, A., Abramovič, H., Poklar Ulrih, N. & Daglia, M. (2020) 'Tea catechins', in *Handbook of Dietary Phytochemicals*. Springer, pp. 1–46.

Bu, Y., Fan, M., Sun, C., Zhu, W., Li, J., Li, X. & Zhang, Y. (2024) 'Study on the interaction mechanism between (−)-epigallocatechin-3-gallate and myoglobin: Multi-spectroscopies and molecular simulation', *Food Chemistry*, 448, p. 139208. doi:10.1016/j.foodchem.2024.139208.

Cano, A., Ettcheto, M., Chang, J.-H., Barroso, E., Espina, M., Kühne, B.A., Barenys, M., Auladell, C., Folch, J. & Souto, E.B. (2019) 'Dual-drug loaded nanoparticles of epigallocatechin-3-gallate (EGCG)/ascorbic acid enhance therapeutic efficacy of EGCG in a APPswe/PS1dE9 Alzheimer's disease mice model', *Journal of Controlled Release*, 301, pp. 62–75. doi:10.1016/j.jconrel.2019.03.010.

Chaachouay, N. & Zidane, L. (2024) 'Plant-derived natural products: a source for drug discovery and development', *Drugs and Drug Candidates*, 3(1), pp. 184–207. doi:10.3390/ddc3010011.

Chowdhury, U.D., Paul, A. & Bhargava, B. (2023) 'Interaction of the tau fibrils with the neuronal membrane', *Biophysical Chemistry*, 298, p. 107024. doi:10.1016/j.bpc.2023.107024.

Coronel, R., Bernabeu-Zornoza, A., Palmer, C., González-Sastre, R., Rosca, A., Mateos-Martínez, P., López-Alonso, V. & Liste, I. (2023) 'Amyloid precursor protein (APP) regulates gliogenesis and neurogenesis of human neural stem cells by several signaling pathways', *International Journal of Molecular Sciences*, 24(16), p. 12964. doi:10.3390/ijms241612964.

Hida, M., Yasuda, K., Toyokawa, M., Asada-Utsugi, M., Toda, S., Yanagida, N., Takahashi, R., Kinoshita, A. & Maki, T. (2025) 'Amyloidogenic and non-amyloidogenic pathways of amyloid precursor protein processing in oligodendrocytes', *Brain Research*, 1855, p. 149601. doi:10.1016/j.brainres.2025.149601.

Jayawardena, B.M., Azzi, A. & Jones, C.E. (2024) 'Investigating the role of phenylalanine residues for amyloid formation of the neuropeptide neurokinin B', *Biochemical and Biophysical Research Communications*, 705, p. 149732. doi:10.1016/j.bbrc.2024.149732.

Karakuş, N. (2024) 'Revealing the antioxidant properties of alkyl gallates: a novel approach through quantum chemical calculations and molecular docking', *Journal of Molecular Modeling*, 30(12), p. 401. doi:10.1007/s00894-024-06196-5.

Kareem, S.A., Abd, M.Y., Hammood, M.N. & Naser, M.A. (2025) 'Understanding the biochemical basis of Alzheimer's disease: A clinical chemistry approach', *Central Asian Journal of Medical and Natural Science*, 6(3), pp. 938–953. doi:10.17605/cajmns.v6i3.2789.

Khalifa, M.K., Abdel-Sattar, S.A., Amin, O.M., Kohaf, N.A., Zaky, H.S., Abd El-Fattah, M.A., Mohammed, K.H., Badawi, N.M., Mansoor, I. & Eassa, H.A. (2024) 'Effectiveness of epigallocatechin gallate nanoparticles on the in-vivo treatment of Alzheimer's disease in a rat/mouse model: A systematic review', *DARU Journal of Pharmaceutical Sciences*, 32(1), pp. 319–337. doi:10.1007/s40199-023-00494-8.

Lee, M., Yoon, J. & Shin, S. (2019) 'Computational study on structure and aggregation pathway of Aβ42 amyloid protofibril', *The Journal of Physical Chemistry B*, 123(37), pp. 7859–7868.

Li, F., Zhan, C., Dong, X. & Wei, G. (2021) 'Molecular mechanisms of resveratrol and EGCG in the inhibition of Aβ42 aggregation and disruption of Aβ42 protofibril: Similarities and differences', *Physical Chemistry Chemical Physics*, 23(34), pp. 18843–18854.

Li, X., Zhang, Y., Yang, Z., Zhang, S. & Zhang, L. (2024) 'The inhibition effect of epigallocatechin-3-gallate on the co-aggregation of amyloid-β and human islet amyloid polypeptide revealed by replica

exchange molecular dynamics simulations', *International Journal of Molecular Sciences*, 25(3), p. 1636. doi:10.3390/ijms25031636.

Liu, H., Guan, H., He, F., Song, Y., Li, F., Sun-Waterhouse, D. & Li, D. (2024) 'Therapeutic actions of tea phenolic compounds against oxidative stress and inflammation as central mediators in the development and progression of health problems: A review focusing on microRNA regulation', *Critical Reviews in Food Science and Nutrition*, 64(23), pp. 8414–8444. doi:10.1080/10408398.2023.2202762.

Mo, Y., Lei, J., Sun, Y., Zhang, Q. & Wei, G. (2016) 'Conformational ensemble of hIAPP dimer: Insight into the molecular mechanism by which a green tea extract inhibits hIAPP aggregation', *Scientific Reports*, 6(1), p. 33076.

Nirmalraj, P.N., Bhattacharya, S. & Thompson, D. (2024) 'Accelerated Alzheimer's Aβ-42 secondary nucleation chronologically visualized on fibril surfaces', *Science Advances*, 10(43), p. eadp5059. doi:10.1126/sciadv.adp5059.

Pan, S.-Y., Nie, Q., Tai, H.-C., Song, X.-L., Tong, Y.-F., Zhang, L.-J.-F., Wu, X.-W., Lin, Z.-H., Zhang, Y.-Y. & Ye, D.-Y. (2022) 'Tea and tea drinking: China's outstanding contributions to the mankind', *Chinese Medicine*, 17(1), p. 27. doi:10.1186/s13020-022-00571-1.

Paroni, G., Bisceglia, P. & Seripa, D. (2019) 'Understanding the amyloid hypothesis in Alzheimer's disease', *Journal of Alzheimer's Disease*, 68(2), pp. 493–510. doi:10.3233/JAD-180802.

Sedov, I. & Khaibrakhmanova, D. (2022) 'Molecular mechanisms of inhibition of protein amyloid fibril formation: Evidence and perspectives based on kinetic models', *International Journal of Molecular Sciences*, 23(21), p. 13428. doi:10.3390/ijms232113428.

Segura, L., Santos, N., Flores, R., Sikazwe, D., McGibbon, M., Blay, V. & Cheng, K.H. (2024) 'Exploring tau fibril-disaggregating and antioxidating molecules binding to membrane-bound amyloid oligomers using machine learning-enhanced docking and molecular dynamics', *Molecules*, 29(12), p. 2818. doi:10.3390/molecules29122818.

Straasø, L.A., Nielsen, J.T., Bjerring, M., Khaneja, N. & Nielsen, N.C. (2014) 'Accurate measurements of 13C-13C distances in uniformly 13C-labeled proteins using multi-dimensional four-oscillating field solid-state NMR spectroscopy', *The Journal of Chemical Physics*, 141(11).

Wang, G., Zhu, X., Song, X., Zhang, Q. & Qian, Z. (2022) 'Melatonin inhibits hIAPP oligomerization by preventing β-sheet and hydrogen bond formation of the amyloidogenic region revealed by replica-exchange molecular dynamics simulation', *International Journal of Molecular Sciences*, 23(18), p. 10264. doi:10.3390/ijms231810264.

World Health Organization (WHO) (2021) *Global status report on the public health response to dementia*. Available at: https://www.who.int/publications/i/item/9789240033245 (Accessed: [insert date]).

Xie, A., Gao, J., Xu, L. & Meng, D. (2014) 'Shared mechanisms of neurodegeneration in Alzheimer's disease and Parkinson's disease', *BioMed Research International*, 2014(1), p. 648740. doi:10.1155/2014/648740.

Xu, Q., Ma, Y., Sun, Y., Li, D., Zhang, X. & Liu, C. (2023) 'Protein amyloid aggregate: Structure and function', *Aggregate*, 4(4), p. e333. doi:10.1002/agt2.333.

Xue, S., Tan, W., Mao, S., Pan, H., Ye, X., Donlao, N. & Tian, J. (2025) 'Polyphenol-based functional materials: Structural insights, composite strategies, and biomedical applications', *Advanced Science*, p. e08924. doi:10.1002/advs.202508924.

Zhang, S., Zhu, Q., Chen, J.-Y., OuYang, D. & Lu, J.-H. (2020) 'The pharmacological activity of epigallocatechin-3-gallate (EGCG) on Alzheimer's disease animal model: A systematic review', *Phytomedicine*, 79, p. 153316. doi:10.1016/j.phymed.2020.153316.

Zhu, J., Negahban, M., Xu, J., Xia, R. & Li, Z. (2023) 'Theoretical analysis of piezoelectric semiconductor thick plates with periodic boundary conditions', *Micromachines*, 14(12), p. 2174. doi:10.3390/mi14122174.

Zvěřová, M. (2019) 'Clinical aspects of Alzheimer's disease', *Clinical Biochemistry*, 72, pp. 3–6. doi:10.1016/j.clinbiochem.2019.04.015.